translations $\mathbf{b}_i$ and given by:

$$\mathbf{b}_i = \sum_j T_{ji}\mathbf{a}_j \,. \qquad (12)$$

Transformation (12) shows that, if **S** is a matrix that transforms the original lattice into a superlattice with determinant |**S**|, then the transpose of matrix **T** is the matrix that transforms the original lattice into a sublattice with determinant $1/|\mathbf{S}|$. Matrices for obtaining sublattices with determinants $\frac{1}{2}, \frac{1}{3}, \frac{1}{4}$ can be obtained by taking the transpose of the inverse of the matrices reported in Table 1. As in the case of superlattices, each set of matrices generating sublattices must be applied to the same primitive cell of the original lattice, but the choice of this cell is arbitrary.

The transformation matrices needed for obtaining composite lattices from the original lattice can be found by multiplying, in any order and in any combination, matrices generating superlattices with matrices generating sublattices. Two simple examples of such matrices are

$(100/020/001) \,.\, (\frac{1}{2}00/010/001) = (\frac{1}{2}00/020/001) \quad |\mathbf{S}| = 1$

and

$(100/0\frac{1}{4}0/001) \,.\, (200/010/001) = (200/0\frac{1}{4}0/001) \quad |\mathbf{S}| = \frac{1}{2}.$

In the first example, the composite lattice is obtained by halving the $\mathbf{a}_1$ axis of the original cell and by doubling the $\mathbf{a}_2$ axis, and the determinant of the transformation is equal to one. In the second transformation, the $\mathbf{a}_1$ axis is doubled and the $\mathbf{a}_2$ axis is reduced to $\frac{1}{4}$ of the original length. The number of composite lattices that can be produced for any given value of the determinant of the transformation is unlimited. For example, composite lattices with $|\mathbf{S}| = 1$ can be obtained in a great variety of ways, such as by combining transformations with determinants 3 and $\frac{1}{3}$, or 2 and $\frac{1}{2}$, or 3, $\frac{1}{2}$, 2 and $\frac{1}{3}$, *etc.* So far we have made no attempt to classify these lattices or to determine their properties. Work on this subject, however, is planned.

References

BUERGER, M. J. (1946). *J. Chem. Phys.* **15**, 1.

BUERGER, M. J. (1954). *Proc. Nat. Acad. Sci. U.S.* **40**, 125.

CASSELS, J. W. S. (1959). *An Introduction to the Geometry of Numbers*. New York: Springer Verlag.

DONNAY, G., DONNAY, J. D. H. & KULLERUD, G. (1958). *Amer. Miner.* **43**, 228.

FRIEDEL, G. (1964). *Leçons de Cristallographie*. Paris: Blanchard.

International Tables for X-ray Crystallography (1969). Vol. I. Birmingham: Kynoch Press.

NIGGLI, P. (1928). *Handbuch der Experimentalphysik*, Vol. 7, Part 1. Leipzig: Academische Verlagsgesellschaft.

Acta Cryst. (1972). A**28**, 287

The Resolution Function of a Slow Neutron Rotating-Crystal Time-of-Flight Spectrometer. II. Application to the Measurement of General Frequency Spectra

BY A. FURRER

Delegation für Ausbildung und Hochschulforschung am Eidg. Institut für Reaktorforschung, 5303 *Würenlingen, Switzerland*

(*Received* 7 *September* 1971)

The resolution function of a slow neutron rotating-crystal time-of-flight spectrometer applied to the measurement of general frequency spectra is treated analytically. It is demonstrated that every component of the instrument may contribute to the uncertainty of the time-of-flight measurement. Focusing conditions are derived, leading to the concept of removable and irremovable time-of-flight spreads. Experimental evidence is presented to support the resolution functions, calculated on the basis of this theory.

1. Introduction

In all neutron-scattering experiments, the observed spectra, $I(\mathbf{Q},\omega)$, are given by the convolution integral

$$I(\mathbf{Q},\omega) = \iint R(\mathbf{Q}'-\mathbf{Q},\omega'-\omega)\sigma(\mathbf{Q}',\omega')\mathrm{d}\mathbf{Q}'\mathrm{d}\omega', \quad (1.1)$$

where $R(\mathbf{Q},\omega)$ is the instrumental resolution function and $\sigma(\mathbf{Q},\omega)$ is the unknown scattering cross section. **Q** and ω are defined by the momentum transfer:

$$\hbar\mathbf{Q} = \hbar(\mathbf{k}_{12}-\mathbf{k}_{23}) \,, \qquad (1.2)$$

and by the energy transfer:

$$\hbar\omega = \frac{\hbar^2}{2m}(\mathbf{k}_{12}^2-\mathbf{k}_{23}^2) \,, \qquad (1.3)$$

in which m denotes the neutron mass. The indices 0,1,2,3 refer to the different spectrometer elements,

i.e. neutron source, monochromator system, sample, and analyser system respectively. Intermediate elements such as flight paths, L, and neutron wave vectors, $\mathbf{k}$, have double indices. In order to obtain precise experimental data, the resolution function has to be known exactly. Moreover, focusing conditions should be such as to optimize the instrumental resolution. The most accurate method of determining $R(\mathbf{Q},\omega)$ would be a direct measurement requiring no prior knowledge of instrumental parameters. This, however, is usually impossible except for zero energy transfer, so that in general $R(\mathbf{Q},\omega)$ has to be calculated. In an earlier paper (Furrer, 1971), which will be referred to as paper I, this was done analytically for a slow neutron rotating-crystal time-of-flight spectrometer applied to phonon measurements. It turned out that the resolution function is dependent upon the geometrical situation in real space. To take account of these geometry effects, it was useful to pursue all possible neutron flight paths in real space and to describe the instrumental resolution as a function of the flight time T.

The present paper contains an analytical treatment of the resolution function of a slow neutron rotating-crystal time-of-flight spectrometer applied to the measurement of general frequency spectra. A general frequency spectrum can be approximated by the superposition of a slowly varying background and several peaks located at different frequencies, ω_i. Resolution and focusing effects only become important at the peak positions. Two approximations are made: (1) for mathematical simplicity, the true peaks are replaced by δ-functions, which is a good approximation whenever the peak shape is symmetrical and $d\omega \ll \omega_i$ (where $d\omega$ denotes the peak width); (2) since in general the scattering cross section, $\sigma(\mathbf{Q},\omega)$, varies slowly as a function of the scattering vector, $\mathbf{Q}$, the detailed $\mathbf{Q}$-dependence of $\sigma(\mathbf{Q},\omega)$ is neglected. Thus we have

$$\sigma(\mathbf{Q},\omega)=\sigma(\omega)=\sum_i \delta(\omega-\omega_i)\,. \tag{1.4}$$

The investigation of $R(\mathbf{Q},T)$ is now reduced to calculating the one-dimensional resolution function $R(T)$, which could be obtained on the basis of the expressions derived in paper I by describing the dispersion surfaces of the frequency spectra as planes $\omega_i=$constant; however, we would have to make use of the scattering surface formalism, which is rather cumbersome for the simplified frequency spectra defined by equation (1.4). Instead of that we present in this paper a more direct way of obtaining the instrumental resolution function.

We shall use the same notation as in paper I. It is shown that every component of the spectrometer contributes to the uncertainty of the time-of-flight measurement. Methods of reducing this uncertainty and thereby obtaining optimum focusing are investigated. This gives rise to a separation into *removable* and *irremovable* time-of-flight uncertainties. The following three assumptions are made. (1) The variation of the flight paths (L) due to the vertical dimension of the monochromator, of the sample and of the detector is ignored. However, this approximation has only a negligible influence on the instrumental resolution function, because the flight paths of a time-of-flight spectrometer are very much longer than the vertical dimensions mentioned above. (2) Since, in a first approximation, the wave number and the direction of the neutron beam are correlated only with respect to its horizontal divergence, the vertical spread of the neutron beam can be ignored. (3) Since the transmission functions of collimators and the mosaic spreads of single crystals are well approximated by Gaussian functions, the shape of the instrumental resolution function is also Gaussian and will be described by its half-width. However, it is not difficult to extend the present investigation to include the exact shape of the resolution function.

Expressions for the removable time-of-flight uncertainties are given in §2. The corresponding focusing conditions arise from the time-dependent incident neutron wave-number distribution, g_{12}, which gives a start advantage to the slower neutrons relative to the faster ones, as well as from the Doppler effect. In §3, the irremovable contributions to $R(T)$ resulting from g_{12} and from the thickness of both the sample and the detector are considered. In §4, calibration experiments are proposed to determine the instrumental parameters. Some experimental results are also presented to illustrate and support the present resolution theory. Some final conclusions are given in §5.

2. Removable time-of-flight uncertainties

2.1. *Monochromator ellipsoid*

In paper I the wave-number distribution g_{12} of the neutrons emitted from the monochromator has been calculated and illustrated for several sets of instrumental parameters. Due to its ellipsoidal form it has been called the *monochromator ellipsoid.* Neglecting the vertical spread, it is given by:

$$\begin{aligned} g_{12}(k'_{12},\gamma_{12},t)\sim\exp\Big\{&-\frac{4\ln 2}{\alpha_{01}^2}\left[\gamma_{12}-2\left(1-\frac{k'_{12}}{k_{12}}\right)\operatorname{tg}\theta_1\right]^2\\ &-\frac{4\ln 2}{\xi_1^2}\left[\gamma_{12}-\left(1-\frac{k'_{12}}{k_{12}}\right)\operatorname{tg}\theta_1\right.\\ &\left.-2\pi\left(\nu t-\frac{u}{w}\right)\right]^2-\frac{4\ln 2}{\alpha_{12}^2}\gamma_{12}^2\Big\}, \end{aligned} \tag{2.1}$$

where k'_{12} denotes the wave number of a particular neutron, γ_{12} is the divergence angle with respect to the optimum emission direction, α is the half-width of the collimator transmission function, ξ_1 is the half-width of the monochromator mosaic spread, θ_1 is the Bragg angle of neutrons emitted with the optimum wave number k_{12}, ν is the spin velocity of the rotating crystal, w is the number of reflecting planes of the monochromator, and u is an integer index denoting the number of neutron bursts already emitted at the time

t. Focusing effects become possible due to the asymmetric distribution of wave numbers k'_{12} relative to the mean emission time, *i.e.* if the monochromator rotation is chosen such that the reflecting planes reach the Bragg position with decreasing angle, the slower neutrons get a start advantage relative to the faster ones.

The flight times for different wave number pairs (k_{12},k_{23}) and (k'_{12},k'_{23}) are given by:

$$T=\frac{m}{\hbar}\left(\frac{L_{12}}{k_{12}}+\frac{L_{23}}{k_{23}}\right) \tag{2.2a}$$

and

$$T'=\frac{m}{\hbar}\left(\frac{L_{12}}{k'_{12}}+\frac{L_{23}}{k'_{23}}\right)+\Delta T', \tag{2.2b}$$

where k_{23} and k'_{23} are obtained from equation (1.3). $\Delta T'$ denotes the emission delay, which is calculated from equation (2.1) by searching the maximum of g_{12} for fixed values of k'_{12}:

$$\Delta T'=-\frac{\alpha_{01}^2-\alpha_{12}^2}{2\pi v(\alpha_{01}^2+\alpha_{12}^2)}\left(1-\frac{k'_{12}}{k_{12}}\right)\operatorname{tg}\theta_1 . \tag{2.3}$$

The corresponding divergence angle turns out to be

$$\gamma_{12}=\frac{2\alpha_{12}^2}{\alpha_{01}^2+\alpha_{12}^2}\left(1-\frac{k'_{12}}{k_{12}}\right)\operatorname{tg}\theta_1 . \tag{2.4}$$

Subtracting (2.2*b*) from (2.2*a*) and combining equations (2.1), (2.3) and (2.4) with $g_{12}=0{\cdot}5$ yields in a first approximation the time-of-flight spread:

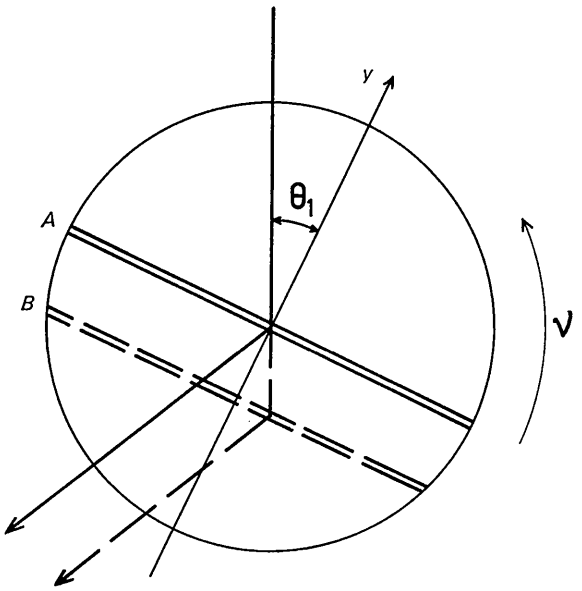

Fig. 1. Schematic sketch of the rotating monochromator. The reflecting planes are parallel to the y axis, which is perpendicular to the bisector of the incoming and outgoing neutron beam. Planes perpendicular to y (*e.g.* the planes A and B) scatter neutrons simultaneously with equal velocities.

$$\delta_1 T=\left[\frac{\alpha_{01}^2-\alpha_{12}^2}{2\pi v(\alpha_{01}^2+\alpha_{12}^2)}-\frac{m}{\hbar}\left(\frac{L_{12}}{k_{12}}+\frac{L_{23}k_{12}^2}{k_{23}^3}\right)\operatorname{ctg}\theta_1\right]\frac{\sqrt{(\alpha_{01}^2+\alpha_{12}^2)}}{4}. \tag{2.5}$$

2.2. *Doppler effect*

Meister (1967) showed that neutron reflexion by a rotating single crystal leads to a space-dependent shift of the reflected neutron velocity and of the reflexion time, which can be expressed as linear functions of the coordinate y, indicated in Fig. 1. In a first approximation, these shifts are given by

$$k_{12}^B-k_{12}^A=\frac{2\pi vmy\sin\theta_1}{\hbar}, \tag{2.6}$$

and

$$\Delta T^B=\frac{my\cos\theta_1}{\hbar k_{12}^A}. \tag{2.7}$$

The sense of monochromator rotation has to be chosen so that the faster neutrons get an emission delay relative to the slower ones; thus it is possible to compensate the shorter flight time as well as the longer flight path due to the monochromator thickness.

The neutron flight times, T_A and T_B, for different reflecting planes, A and B, of the monochromator are given by:

$$T_A=\frac{m}{\hbar}\left(\frac{L_{12}}{k_{12}^A}+\frac{L_{23}}{k_{23}^A}\right) \tag{2.8a}$$

and

$$T_B=\frac{m}{\hbar}\left(\frac{L_{12}+y/\cos\theta_1}{k_{12}^B}+\frac{L_{23}}{k_{23}^B}\right)+\Delta T^B. \tag{2.8b}$$

Using equations (2.6), (2.7) and (2.8) one obtains in a first approximation the time-of-flight spread:

$$\delta_2 T=\frac{2\pi vm^2 y\sin\theta_1}{\hbar^2}\left[\frac{L_{12}+y/\cos\theta_1}{k_{12}^2}+\frac{L_{23}k_{12}}{k_{23}^3}\right]-\frac{my}{\hbar k_{12}}\left(\frac{1}{\cos\theta_1}+\cos\theta_1\right), \tag{2.9}$$

where y takes the values $\frac{r\sqrt{3}}{2}$ and $\frac{r\sqrt{2}}{2}$ for monochromator crystals of cylindrical and spherical shape, respectively, in which r denotes the crystal radius.

2.3. *Focusing procedure*

The idea of focusing consists of minimizing the individual time-of-flight spreads, $\delta_1 T$ and $\delta_2 T$, defined by equations (2.5) and (2.9). Seven independent parameters have to be determined by a minimization procedure: $k_{12},\theta_1,L_{12},L_{23},\alpha_{01},\alpha_{12},v$. However, the calculation often yields parameter values that are unreasonable because of instrumental restrictions. Thus a rigorous mathematical treatment will not be successful in general, and a semi-empirical method has to be applied.

Equation (2.5) shows that efficient focusing can be obtained for large values of θ_1 and $(\alpha_{01}^2-\alpha_{12}^2)$. However, in most cases it is impossible to remove $\delta_1 T$ completely, since the first term in the square brackets is much smaller than the second one. L_{12}, L_{23}, and v are the appropriate parameters to minimize $\delta_2 T$. Here, the positive and negative terms have the same order of magnitude, so that $\delta_2 T$ usually cancels out by a variation procedure. The parameter k_{12} is in general predetermined by intensity and energy resolution considerations and should not be used for generating focusing effects.

3. Irremovable time-of-flight uncertainties

3.1. *Monochromator ellipsoid*

In §2.1 we calculated the removable part of the time-of-flight uncertainty due to the monochromator ellipsoid. A delay time $\Delta T'$ has been derived for neutrons emitted into the direction defined by γ_{12}, with a fixed wave number, k'_{12}. The irremovable time-of-flight uncertainty arises from neutrons scattered with the same wave number k'_{12}, but with different divergence angles γ_{12}. This time-of-flight spread is independent of k'_{12} and may therefore be calculated for $k'_{12}=k_{12}$. The result derived from equation (2.1) with $g_{12}=0{\cdot}5$ is

$$\delta_3 T=\frac{1}{2\pi v}\sqrt{\frac{\alpha_{01}^2\xi_1^2+\alpha_{01}^2\alpha_{12}^2+\xi_1^2\alpha_{12}^2}{\alpha_{01}^2+\alpha_{12}^2}}. \qquad (3.1)$$

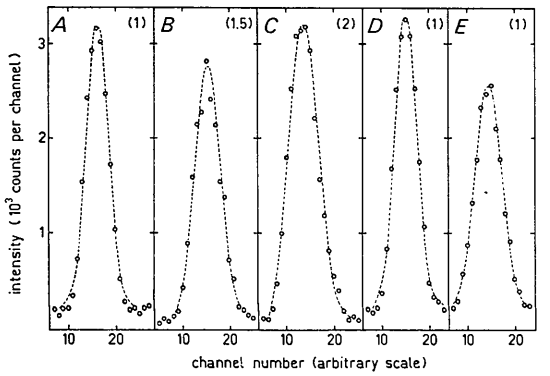

Fig. 2. Observed elastic peaks from time-of-flight spectra for vanadium. The dashed lines correspond to the calculated resolution functions. The numbers in brackets are the factors by which the intensity has been multiplied. The channel width has a value of 8 μsec.

3.2. *Sample thickness*

It has been shown in paper I that curves of constant flight times at the sample position are given by a set of straight lines. The inclination angle relative to the incoming neutron beam is given by:

$$\operatorname{tg}\vartheta=\operatorname{ctg}\psi-\frac{k_{23}}{k_{12}\sin\psi}, \qquad (3.2)$$

where ψ denotes the scattering angle. The uncertainty due to finite sample size is then obtained by a simple integration procedure, provided the whole sample is uniformly irradiated by the neutrons. Using equation (3.2), we get

$$\delta_4 T=\frac{mW_s\sqrt{(k_{12}^2-2k_{12}k_{23}\cos\psi+k_{23}^2)}}{\hbar k_{12}k_{23}}, \qquad (3.3)$$

where W_s is a characteristic length, depending on the shape of the sample. It is equal to $D\,.\sin(\varphi-\vartheta)$ for a plate, $r\sqrt{3}$ for a cylinder, and $r\sqrt{2}$ for a sphere, where r denotes the radius of the cylinder and the sphere, and D the horizontal length of the plate, whose inclination angle is given by φ. Consequently, $\delta_4 T$ vanishes for thin plates positioned in such a manner that $\varphi=\vartheta$.

3.3. *Detector thickness*

The thickness of the counter introduces an uncertainty into the flight path and thus gives rise to an irremovable time-of-flight spread:

Table 1. *Instrumental parameters, calculated and observed widths of the elastic peaks shown in Fig.* 2

The vanadium sample was in the form of a 5·0 × 5·0 × 0·4 cm plate.
The following parameters were held constant: $\alpha_{01}=30'$, $\xi_1=20'$, $r=2$ cm, $\psi=90°$, $\vartheta=-45°$, $L_{23}=200$ cm.

Peak number	*A*	*B*	*C*	*D*	*E*
α_{12}	120′	80′	130′	90′	90′
$\nu(s^{-1})$	200	83	83	200	200
Monochromator	Sphere	Cylinder	Cylinder	Cylinder	Cylinder
L_{12} (cm)	185	300	185	275	275
$k_{12}=k_{23}$ (Å^{-1})	2·34	2·34	2·34	3·92	3·92
θ_1	35°	35°	35°	20°	20°
W_s (cm)	0·4	0·4	0·4	0·4	5·0
φ	− 45°	− 45°	− 45°	− 45°	+ 45°
W_d (cm)	1·55	1·55	1·55	1·84	1·84
$\delta_1 T$ (μsec)	39·8	39·1	52·8	40·8	40·8
$\delta_2 T$ (μsec)	1·5	12·0	14·7	8·2	8·2
$\delta_3 T$ (μsec)	8·1	19·2	19·7	8·0	8·0
$\delta_4 T$ (μsec)	3·8	3·8	3·8	2·3	28·6
$\delta_5 T$ (μsec)	10·5	10·5	10·5	7·4	7·4
Γ_r (μsec)	42·2	46·6	59·3	43·1	51·7
Γ_{exp} (μsec)	41·5 ± 1·3	48·7 ± 2·5	57·1 ± 3·0	42·0 ± 1·6	51·6 ± 1·6

$$\delta_5 T = \frac{m W_d}{\hbar k_{23}}, \tag{3.4}$$

where W_d is equal to the half-width of the response probability of the counter, depending on the shape and size of the detector, on the absorption properties and pressure of the filling gas, and on the wave number, k_{23}. This has been shown in paper I, where W_d is presented as a function of radius, gas pressure, and neutron energy for a cylindrical ^{3}He detector.

4. Experimental results

The half-width of the instrumental resolution function $R(T)$ is given by

$$\Gamma_r = \sqrt{\left[\sum_{i=1}^{5} (\delta_i T)^2 \right]}, \tag{4.1}$$

where the individual contributions $\delta_i T$ have been defined in §2 and §3. The calculation of Γ_r requires a precise knowledge of the instrumental parameters, $\alpha_{01}, \alpha_{12}, \xi_1, y, W_s, W_d$, whose values should preferably be determined experimentally. Such calibration experiments are carried out by observing the incoherent elastic scattering from the sample at various Bragg angles θ_1, neutron wave-numbers k_{12}, flight paths L_{12} and L_{23} and speeds of rotation ν. The set of resolution functions thus obtained for zero energy transfer may then be used to adapt the instrumental parameters, with the aid of a variational procedure. For these calibration experiments, it is important to use a sample whose coherent scattering contributions are negligibly small, in order to prevent additional broadening arising in the vicinity of the Bragg positions.

Formula (4.1) is now examined by means of experimental peaks obtained with a vanadium sample at different spectrometer settings that have not previously been used for the calibration experiments. The results are shown in Fig. 2 for the particular instrumental parameters given in Table 1. The experimental peaks indeed confirm the assumed Gaussian shape of the resolution functions. The calculated and observed widths always agree within the experimental error. No experimental evidence can be given for the general case of inelastic peaks. However, this should not reduce the confidence in the present resolution theory, since the resolution contributions (2.5), (2.9) and (3.3) contain the change from elastic to inelastic processes in a straightforward manner.

5. Discussion

By introducing the concept of removable and irremovable time-of-flight spreads, the resolution function and the focusing conditions of a rotating-crystal time-of-flight spectrometer have been treated quantitatively for the measurement of general frequency spectra. To derive the unknown scattering cross-section, it has been assumed that the resolution function does not change over the small range $d\omega$ given by the finite peak widths of the frequency spectrum. In general, the rotating-crystal time-of-flight spectrometer covers a large frequency range for one single instrumental configuration, but the focusing conditions are such that only part of this range can be observed with optimum resolution. If one is mainly interested in line widths, a single frequency spectrum must therefore be measured several times with different spectrometer settings adapted to the respective frequency transfers. However, this is not a specific disadvantage of a time-of-flight spectrometer.

Two quantities are of interest for planning actual experiments: the energy resolution rather than the absolute instrumental resolution Γ_r defined by equation (4.1) and the intensity. The energy resolution is given by

$$\frac{dE}{E} = \frac{2\hbar k_{23}^2}{m L_{23}(k_{12}^2 - k_{23}^2)} \Gamma_r, \tag{5.1}$$

where E denotes the energy transfer defined in equation (1.3). By integrating equation (2.1) over k'_{12}, γ_{12}, and t, the intensity turns out to be

$$I \sim A(\xi_1, \nu) w \alpha_{01} \xi_1 \alpha_{12} k_{12} \operatorname{ctg} \theta_1 . \tag{5.2}$$

Herein, $A(\xi_1, \nu)$ takes account of the neutron storage effect described by Carvalho, Ehret & Gläser (1967).

It is worthwhile mentioning here that the procedure described in this paper can easily be adapted to a randomly pulsed experiment, as well as to a spectrometer at a pulsed neutron source.

I wish to acknowledge the stimulating discussions with my colleagues of the slow neutron scattering group at Würenlingen.

References

CARVALHO, F., EHRET, G. & GLÄSER, W. (1967). *Nucl. Instrum. Methods*, **49**, 197.
FURRER, A. (1971). *Acta Cryst.* A**27**, 461.
MEISTER, H. (1967). *Nukleonik*, **10**, 97.